

# 1 The quest for fusion power

This chapter introduces the basic physics and associated variables. Except for those variables cited at the foot of page XVI, SI units are almost always adopted. Pages XV and XVI have lists of physical constants, plasma parameters and frequently used symbols.

## 1.1 Tokamak machines

### 1.1.1 Topology and ignition

A tokamak is a toroidal chamber which uses a strong toroidal magnetic field,  $B_\varphi$ , to contain a high temperature plasma within the torus. Charged particles cannot easily move across strong magnetic fields and if the fields are closed into nested surfaces, then deuterium and tritium ions trapped in this way and colliding with sufficient energy to overcome their repulsive Coulomb potential, will fuse and liberate energy. The toroidal field is produced by external electric currents flowing in coils wound around the torus, as shown in Fig. 1.1. Superimposed on the toroidal field is a much weaker poloidal field,  $B_\theta$ , generated by an electric current  $I_p$  flowing in the plasma around the torus. The plasma forms the secondary circuit of a transformer, so that  $I_p$  is induced by changing the magnetic flux  $B_T$  passing through the torus, which is usually carried by an iron core as indicated in the figure.

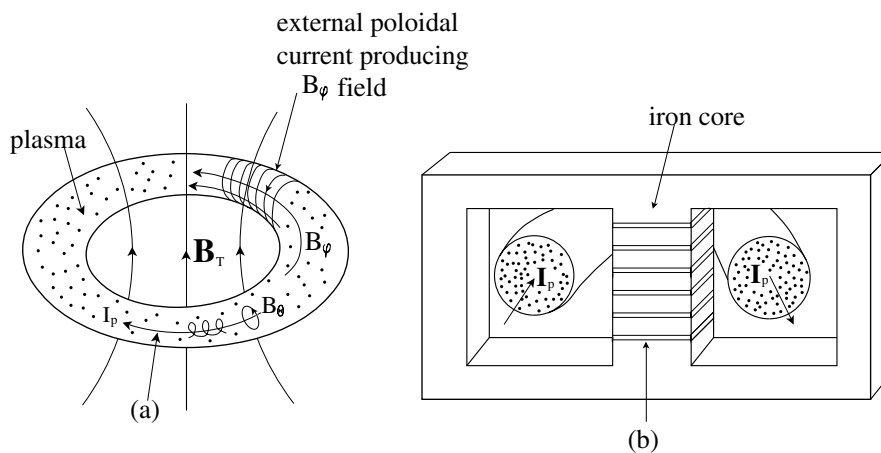
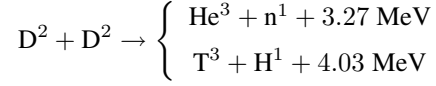
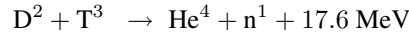
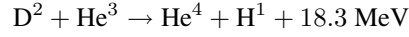


**Figure 1.1:** Tokamak currents and fields: (a) toroidal plasma current induced by transformer, (b) primary winding

In a plasma consisting of deuterium, or deuterium mixed with tritium, the fusion reactions



and



will occur frequently if the ion temperature,  $T_i$ , and the ion number density,  $n_i$ , are large enough. Furthermore, in a *fusion reactor* these high values of  $T_i$  and  $n_i$  must be maintained long enough for the energy liberated by fusion to more than balance the energy losses due to radiation, conduction, convection and neutron flux. Let  $\tau_E$  be the time it takes these loss processes to remove all the energy from the system, then for a given value of  $n_i\tau_E$  there is a minimum temperature at which the plasma is said to *ignite*, i.e. at which the liberated fusion energy is just adequate to balance all losses. As D-D plasmas require considerably higher temperatures to achieve ignition, almost all reactor proposals have concentrated on D-T fusion.

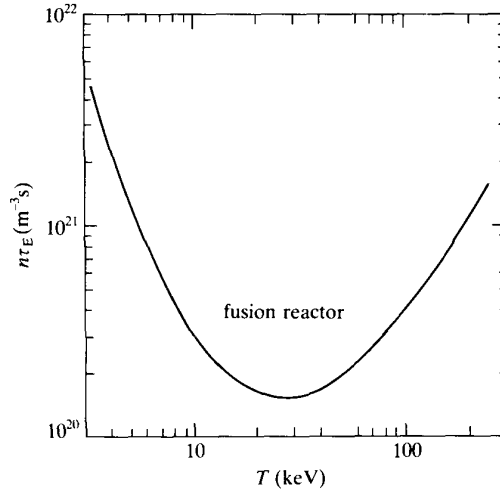


**Figure 1.2:** Ignition curve for a D-T plasma

Figure 1.2 shows the ignition curve for a D-T plasma. It has a minimum at a temperature of about 30 keV, where for ignition we need  $n_i\tau_E > 1.5 \times 10^{20} \text{ m}^{-3}\text{s}$ . A slightly lower bound ( $n_i\tau_E > 6 \times 10^{19} \text{ m}^{-3}\text{s}$ ) known as Lawson's criterion (Lawson 1957) is obtained if a continuous power supply from outside the system is used to compensate transport and radiation losses. Combining the  $n_e\tau_E$  value with  $\hat{T} \sim 10 \text{ keV}$ , we obtain

$$\tau_E n_i \hat{T} > 3 \times 10^{21} \text{ s m}^{-3} \text{ keV}, \quad (1.1)$$

which is based on the assumption that the number density and temperature profiles across the minor radius are flat. When allowance is made for typical profile shapes, and the constraint is applied to the peak values,  $T_0$  and  $n_{i0}$  of the temperature and number density profiles, (1.1) is replaced by

$$\tau_E n_{i0} \hat{T}_0 > 5 \times 10^{21} \text{ s m}^{-3} \text{ keV}.$$

Observations show that electron energy losses are dominant and in a pure D-T plasma, by charge neutrality,  $n_i = n_e$ , and so to a good approximation the left-hand side of (1.1) can be replaced by  $\tau_{Ee} n_e \hat{T}_e$ .

Let  $B$  denote the strength of the magnetic field<sup>1</sup>, then for a reason explained in the first of the plasma physics notes in the Appendix,  $B^2/2\mu_0$  is called the magnetic pressure, where  $\mu_0$  is the free-space permeability. An important parameter in plasma physics is the ratio of the plasma pressure  $p$  to the magnetic pressure, which is known as the plasma *beta*,

$$\beta \equiv \frac{2\mu_0 p}{B^2}. \quad (1.2)$$

The power output for a given magnetic field and plasma assembly is proportional to the square of beta, and for an adequate return on an energy investment in magnetic fields, it has been estimated that in a reactor  $\beta$  should exceed 0.1.

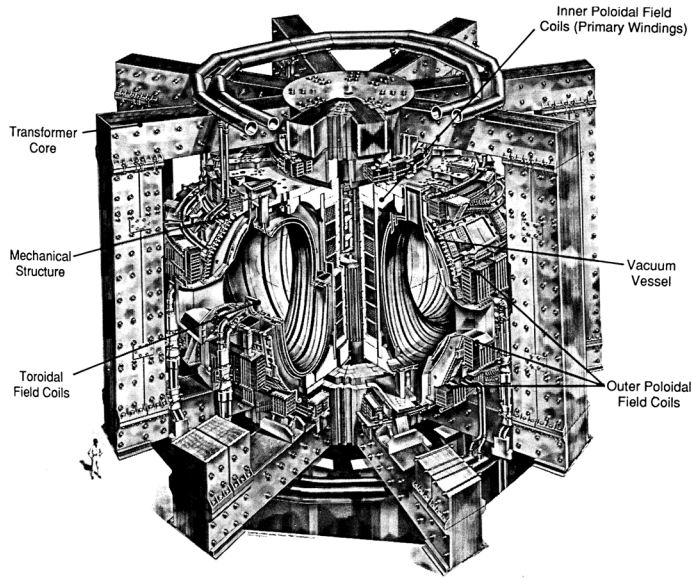


**Figure 1.3:** The Joint European Torus (JET)

<sup>1</sup>Strictly the magnetic *induction*, but the misnomer ‘field’ is commonly adopted in plasma physics.

### 1.1.2 Some early tokamaks

The advantage of the Russian tokamak machine over similar toroidal devices that were being developed in the United States and Great Britain at the same time, lay in the better stability obtained by using much stronger toroidal magnetic fields. ‘Stability’ in this context means no more than the persistence of the magnetic fields and electric currents — at least in the earlier machines — for times of the order of milliseconds. The British ZETA machine, which received much publicity in the 1950s, was so-called ‘stable’ for less than about 5 milliseconds, whereas the discharge in comparable tokamaks lasted over ten times longer.

In his review of the history of tokamak research from 1955 to 1980, Rutherford (1980) noted that this confinement device was responsible for more than half the articles published in the specialist journal *Nuclear Fusion*. The first substantial tokamak was T-3, built at the Kurchatov Institute, Moscow in the 1960s. It had a minor radius of 15 cm, a major radius of 100 cm, a toroidal magnetic field of 15 kG, and carried a plasma current of 100–250 kA. In the standard notation (see Fig. 1.4),  $a = 0.15$  m,  $R_0 = 1$  m,  $B_\varphi = 1.5$  T,  $\hat{I}_p = 0.1 - 0.25$  MA.

Some twenty years later the Joint European Torus (JET) was constructed at a cost of around £200 M on the Culham site at Abingdon, England, and this is currently the largest tokamak in the world. The cross-section of the torus in JET is D-shaped, with a (horizontal) width of 2.4 m and a height of 4.2 m. Its parameters are:  $a = 1.2 \times 2.1$  m,  $R_0 = 3$  m,  $B_\varphi = 3.5$  T,  $\hat{I}_p = 5$  MA. Whereas T-3 reached electron temperatures  $\sim 0.4 - 1.0$  keV and ion temperatures  $\sim 0.2$  keV at average electron number densities of  $\bar{n}_e \sim 2 \times 10^{19} \text{ m}^{-3}$  and energy confinement times of only a few milliseconds, by 1986 JET had achieved  $T_e \sim 6$  keV,  $T_i \sim 12$  keV,  $\bar{n}_e \sim 3.5 \times 10^{19} \text{ m}^{-3}$  and  $\tau_E \sim 0.9$  s, although not simultaneously. However, from (1.1) increases by factors of 3 in  $T_i$  and 5 in  $n_i \tau_E$  were still required for ignition.

Wesson (2004) gives details of forty-four tokamaks built up to 1985 in England, France, Germany, Italy, Japan, USA, and USSR; Table 1.1 lists those built since 1975. Notice that under the column of the minor radius, DOUBLET III and JET have two lengths written as  $a \times b$  where  $b$  is the half-height of the plasma and  $a$  is the minor radius, or half-width of the plasma; these lengths serve as a rough specification of D-shaped cross sections (e.g. JET’s

**Table 1.1:** Typical values of tokamak parameters (not simultaneous)

| Machine         | year | $R_0$ | $a$                | $B_\varphi$ | $\hat{I}_p$ | $\bar{n}_e$               | $\hat{T}_{e0}$ | $\hat{T}_{i0}$ | $\tau_E$ |
|-----------------|------|-------|--------------------|-------------|-------------|---------------------------|----------------|----------------|----------|
|                 | (m)  |       | (m)                | (T)         | (MA)        | $10^{-19} \text{ m}^{-3}$ | (keV)          | (keV)          | (ms)     |
| DITE            | 1975 | 1.17  | 0.26               | 2.7         | 0.2         | 5                         | 0.7            | 0.6            | 14       |
| PLT             | 1975 | 1.3   | 0.40               | 3.5         | 0.6         | 5                         | 3              | 3              | 40       |
| T-10            | 1975 | 1.5   | 0.37               | 4.5         | 0.5         | 4                         | 1.4            | 0.7            | 50       |
| DOUBLET III     | 1979 | 1.43  | $0.44 \times 0.75$ | 2.4         | 0.9         | 10                        | 4              | 4              | 100      |
| TFTR            | 1982 | 2.4   | 0.80               | 5.0         | 2.2         | 4                         | 2              | 8              | 200      |
| JET             | 1983 | 3.0   | $1.2 \times 2.1$   | 3.5         | 5.0         | 3.5                       | 6              | 8              | 500      |
| TEXTOR          | 1983 | 1.75  | 0.46               | 2.0         | 0.4         | 3                         | 1.2            | 0.8            | 40       |
| JT-60           | 1985 | 3.0   | 0.9                | 4.5         | 2.0         | 7                         | 3              | 5              | 100      |
| DIII-D          | 1986 | 1.67  | 0.67               | 2.1         | 5.0         | 8                         | 26             | 20             | 160      |
| ASDEC (upgrade) | 1991 | 1.65  | 0.50               | 3.9         | 1.4         | 11                        |                |                |          |

vacuum vessel shown in Fig. 1.3). The elongation of the cross-section follows from a solution of the MHD equilibrium equations, which determine the magnetic field structure appropriate for a given choice of pressure and current profiles (Section 2.1). However, in this text to simplify the analysis with relatively little impact on general conclusions concerning transport, the ‘elongation’ variable,  $\kappa = b/a$ , will be taken to be unity.

### 1.1.3 Toroidal current

There is one evident disadvantage in the tokamak design as illustrated in Fig. 1.1, namely that its operation is necessarily pulsed because resistivity will gradually dissipate the inductive current and switch off the discharge. Quite apart from its role in heating the plasma through ohmic dissipation, a toroidal current is essential to maintain an elongated toroidal system in equilibrium, for without the  $B_\theta$  field that it generates, there is a vertical instability that causes the plasma to drift in the direction of elongation. The force driving this instability results from the interaction of the poloidal field coil currents (see Fig. 1.1) and the plasma current. In some cases feedback control circuitry is necessary to maintain the plasma’s position (see Wesson, 2004, p. 342).

Early tokamaks, which relied entirely on inductive currents for both heating and stabilization, were therefore designed for pulsed operation in the hope that the pulse time could be made sufficiently long for fusion to be effective; but these times are measured in seconds rather than minutes and are too short for reactor operation.

Finding other ways of continuously heating the plasma and of maintaining the stabilizing toroidal current, has been an important quest in recent tokamak research. Steady currents can be driven around the torus with radio-frequency (RF) waves and also with neutral beam injection (NBI), but there are limits to this type of ‘current drive’ that make it unable to generate all of the current required for a stable reactor. One such constraint, called the ‘Greenwald’ limit, is concerned with the avoidance of major disruptions (Section 6.2.1). For a survey of NBI current drive the reader is referred to ITER team (1999, p. 2527).

However, there is another mechanism that generates non-inductive toroidal currents. It is widely believed that a large current of this type, termed a ‘bootstrap’ current, can be generated simply by the existence of radial gradients in the plasma density and temperature. Observations certainly support the presence of a non-inductive current, but its origin is not the bootstrap phenomenon, for as shown in Section 3.4.3, such a current does not satisfy Ampère’s law and cannot exist. In Section 5.3.2 we show that the observed non-inductive current is a result of the toroidal electric field generated by the radial flow of the plasma across the  $B_\theta$  magnetic field.

Let  $v_D$  be the radial velocity of the plasma flowing across the tokamak magnetic field, then the toroidal electric field, say  $E_\varphi^{LR}$ , driving the non-inductive current is proportional to the product  $v_D B_\theta$ , so the ‘price’ of this potentially steady current is the continual loss of plasma from the torus. Regular refueling by beam injection near the minor axis is therefore required to maintain the current, a process with its own limitations (see Section 1.4.2).

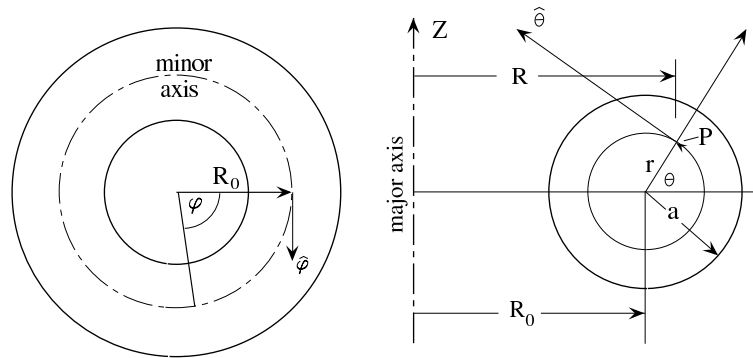


Figure 1.4: Cylindrical and local coordinates for a tokamak machine

## 1.2 Basic tokamak variables

### 1.2.1 Aspect ratio

Figure 1.4 shows the coordinate systems for a tokamak of circular cross-section. The local radial dimension lies in the range  $0 < r < a$ , where  $a$  is the maximum radius of the plasma. In order to prevent the plasma reaching the vacuum vessel, either a material *limiter* or a magnetic *divertor* is used, as shown in Fig. 1.5. Most tokamaks have limiters, but divertors have the merit of reducing the influx of ionized impurities into the interior of the plasma by diverting them into an outer “scrape-off” layer.

The tokamak aspect ratio,  $R_0/a$ , usually lies between 3 and 5 and as we shall see later, it has an important role in plasma energy confinement.

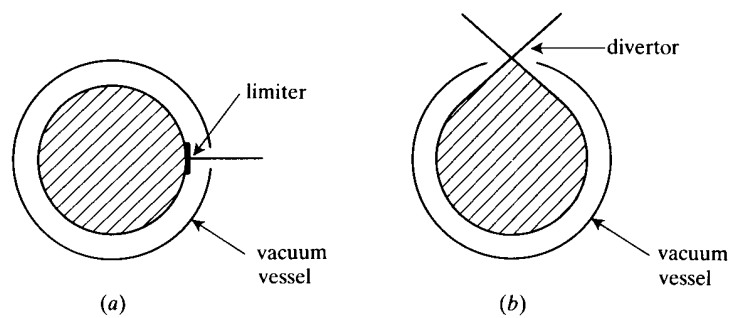


Figure 1.5: Separation of plasma from wall by (a) a limiter, (b) a divertor

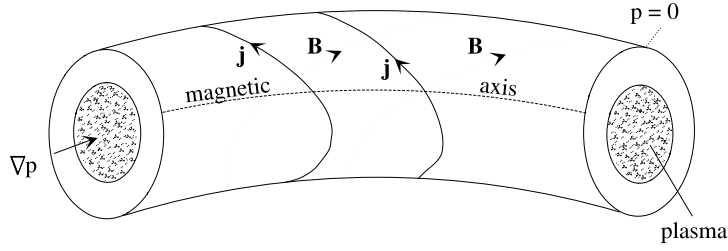


Figure 1.6: Nested magnetic surfaces confining a plasma

### 1.2.2 Beta

Several forms of the ratio of the average plasma pressure to the magnetic field pressure<sup>2</sup> arise in tokamak theory. For simplicity we shall assume that the magnetic surfaces have concentric, circular cross-sections and that conditions are independent of the value of the toroidal variable,  $\varphi$ , defined in Fig. 1.4. To obtain the volume-averaged pressure  $\langle p \rangle$ , we integrate over a cross-section  $\varphi = \text{const.}$ ,

$$\langle p \rangle = \int p dS / \int dS = \frac{2}{a^2} \int_0^a p(r) r dr. \quad (1.3)$$

From the  $\hat{\varphi}$ -component of the differential form of Ampère's law relating the magnetic field vector  $\mathbf{B}$  to the electric current density  $\mathbf{j}$ , viz.  $\nabla \times \mathbf{B} = \mu_0 \mathbf{j}$ , we get

$$\frac{1}{r} \frac{\partial}{\partial r} (r B_\theta) = \mu_0 j_\varphi, \quad B_\theta = \frac{\mu_0}{r} \int_0^r j_\varphi(r') r' dr' \quad (1.4)$$

and

$$I_p = 2\pi \int_0^a j_\varphi r dr = 2\pi a B_{\theta a} / \mu_0, \quad (1.5)$$

where  $I_p$  is the total current flowing around the torus and  $B_{\theta a}$  is the poloidal magnetic field at the limiter,  $r = a$ . In the following we shall assume that small variations in  $B_\varphi$  across the plasma cross-section can be ignored.

In Section A.1 it is shown that in equilibrium configurations,  $\mathbf{B}$  and  $\mathbf{j}$  lie on constant pressure surfaces, which if closed, appear as continuous windings of intersecting magnetic field and current lines; these are said to lie on 'magnetic surfaces' and  $p$  is termed a 'surface quantity'. Figure 1.6 shows a set of nested surfaces, with a limit line at their center, known as the 'magnetic axis'. If  $p$  increases towards the axis, its negative gradient is balanced by the  $\mathbf{j} \times \mathbf{B}$  force directed inwards; the plasma is thus confined by the magnetic force.

<sup>2</sup>See Section A.1, the first of the Plasma Physics Notes, collected in the Appendix and mostly intended for readers not familiar with the equations of plasma physics. The Notes are referenced in the text as Section A.1, Section A.2... and the equations are numbered consecutively throughout the Appendix: (A.1), (A.2),..., (A.100),..., etc.

Functions of importance in tokamak theory are the toroidal beta  $\beta_t$  and the poloidal beta  $\beta_p$ , which are defined by

$$\beta_t = \frac{2\mu_0\langle p \rangle}{B_\varphi^2}, \quad \beta_p = \frac{2\mu_0\langle p \rangle}{B_{\theta a}^2} = \frac{8\pi^2 a^2 \langle p \rangle}{\mu_0 I_p^2}. \quad (1.6)$$

In Section 1.1 we mentioned the connection between  $\beta_t$  and the economic viability of a tokamak reactor, which expressed as a percentage, is  $\beta_t \geq 10\%$ ; this is only a rough estimate of the economic constraint — higher values may be required.

On the other hand, ideal MHD stability imposes an upper limit on  $\beta_t$ . The type of instability involved is termed a ‘ballooning mode’ (see Section 6.3.2), and the outcome are the approximate  $\beta$ -limits,

$$\beta_t \leq 0.15 \frac{a}{R_0 q_a}, \quad \beta_p \leq 0.15 \frac{R_0 q_a}{a} \quad \left( q_a \equiv \frac{a B_\varphi}{R_0 B_{\theta a}} \right),$$

or

$$\beta_N \equiv 20\beta_t \frac{R_0 q_a}{a} = 20\beta_p \frac{a}{R_0 q_a} \leq 3.5, \quad (1.7)$$

where  $\beta_N$  is called the ‘normalized’ beta and  $q_a$  is the safety factor defined in the following section.

### 1.2.3 Safety factor

The safety factor is another important parameter, so named because of its association with stability, as explained in Section A.24. In a large aspect ratio tokamak with a circular cross-section, this parameter is defined by

$$q(r) = \frac{r B_\varphi}{R_0 B_\theta} = \frac{\varepsilon}{s}, \quad (1.8)$$

where

$$\varepsilon \equiv \frac{r}{R_0}, \quad s \equiv \frac{B_\theta}{B_\varphi} = \frac{\mu_0}{B_\varphi r} \int_0^r j_\varphi(r') r' dr'. \quad (1.9)$$

In tokamaks  $s$  is much smaller than unity.

At the limiter by (1.5) and (1.18)  $q$  has the value

$$q_a = \frac{a B_\varphi}{R_0 B_{\theta a}} = \frac{2\pi a^2 B_\varphi}{\mu_0 I_p R_0} = \frac{5a^2 B_\varphi}{\hat{I}_p R_0}, \quad (\hat{I}_p \text{ in MA}). \quad (1.10)$$

Hence the average current density,  $\langle j_\varphi \rangle = I_p / \pi a^2$ , is

$$\mu_0 \langle j_\varphi \rangle = \frac{2B_\varphi}{R_0 q_a}. \quad (1.11)$$

By expanding  $j_\varphi$  in the form  $j_\varphi = j_{\varphi 0} + O(r^2)$ , where  $j_{\varphi 0}$  is the current density on the minor axis, we find from (1.8) and (1.9) that on the magnetic axis ( $r = 0$ ), the safety factor has the value

$$q_0 = \frac{2B_\varphi}{\mu_0 j_{\varphi 0} R_0}. \quad (1.12)$$

From (1.11) and (1.12) we obtain

$$q_a/q_0 = j_{\varphi 0}/\langle j_{\varphi} \rangle, \quad (1.13)$$

hence large values of  $q_a/q_0$  correspond to peaked current profiles.

The general definition of  $q$  is

$$q = \oint \frac{B_{\varphi}}{R_0 B_{\theta}} ds,$$

where the integral is along a closed path enclosing the minor axis and lying on a specific magnetic surface; thus  $q$  is a surface quantity.

### 1.2.4 Z-effective

Tokamaks usually have several types of ion in their plasmas, due mainly to impurities entering from the torus walls, and a convenient measure of the extent to which the plasma is contaminated is the function known as ‘Z-effective’, defined by

$$n_e Z_{\text{eff}} = \sum_s n_s Z_s^2 \quad n_e = \sum_s n_s Z_s,$$

where  $Z_s$  is the charge number for the s-type ion. In a pure hydrogen plasma,  $Z_{\text{eff}} = 1$ , but few tokamaks achieve values even near this ideal. Pfeiffer and Waltz (1979) list 118 observations on 11 early tokamaks. Many of these machines were heavily contaminated, the average  $Z_{\text{eff}}$  being about 5. Initially the JET tokamak had  $Z_{\text{eff}}$  lying in a range extending from above 2 to about 10 (Christiansen et al. 1985). More recently this has dropped to a range from just below 2 to about 3.5.

Figure 1.7, from the JET Team (1990), illustrates the importance of the choice of boundary materials in limiter tokamaks. An empirical law for JET of the type  $Z_{\text{eff}} \propto 1/(n_{i9}^{0.9} q_a^{0.7})$ ,

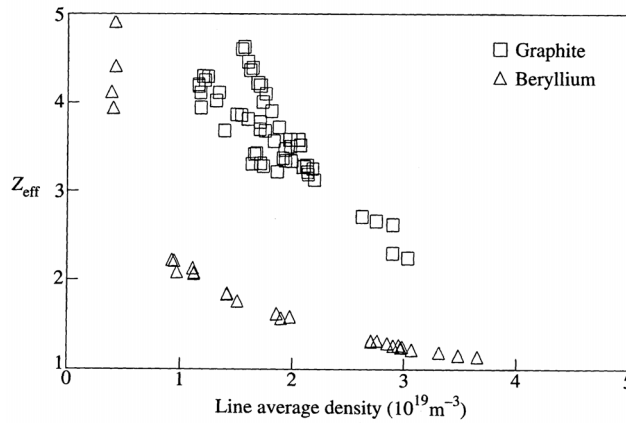


**Figure 1.7:**  $Z_{\text{eff}}$  as a function of density with either graphite or beryllium limiters

where  $n_{19} = n/10^{19}$ , has been found (Cordey et al. 1985b), while Matthews et al. (1997) have compiled a multi-machine data base showing that  $Z_{\text{eff}}$  depends on the radiated energy, the plasma surface area and  $n_e^2$  for all divertor tokamaks, independent of geometry.

Impurity concentrations may be determined by analyzing resonance line intensities in the vacuum UV, supplemented by measurements of soft X-ray spectra; this data, coupled with a theory for ionization rates, enables  $Z_{\text{eff}}$  to be estimated. Another method determines  $Z_{\text{eff}}$  from the visible bremsstrahlung radiation. In JET the two methods yield values for  $Z_{\text{eff}}$  that are usually within  $\pm 1$  of each other. The main impurities in JET are C (2–3 per cent), O (1–4 per cent), Cl and Ni (Denne et al. 1985).

A further method of estimating  $Z_{\text{eff}}$  relies on an application of Spitzer's (1962) formula for the parallel resistivity (see Section A.2). Measurements of the plasma current  $I_p$ , the 'loop' voltage  $V_\ell$  around the torus, and assumptions about the radial distribution of the variables, enables  $Z_{\text{eff}}$  to be calculated from the integral

$$I_p = \int j_\varphi dS = 2\pi \int_0^a \hat{\varphi} \cdot \boldsymbol{\sigma} \cdot (\mathbf{E} + \mathbf{v} \times \mathbf{B}) dr,$$

where  $\boldsymbol{\sigma}$  is the conductivity tensor,  $\mathbf{E}$  is the electric field, and  $\mathbf{v}$  is the plasma velocity. We also need the equation for the electron collision interval (see (A.16) in Section A.2),

$$\tau_e = \frac{2.75 \times 10^5}{\ln \Lambda} \frac{T_e^{3/2}}{n_e Z_{\text{eff}}}, \quad (1.14)$$

and the relation

$$V_t/2\pi R_0 = \hat{\varphi} \cdot (\mathbf{E} + \mathbf{v} \times \mathbf{B}) = E_\varphi + v_r B_\theta, \quad (1.15)$$

defining the total voltage  $V_t$ . It is usual to omit the term  $v_r B_\theta$  compared with  $E_\varphi$ , but this can result in appreciable errors, as will be explained in Section 5.3.2.

An important modification to this method (Christiansen et al. 1985) replaces the parallel conductivity  $\sigma_\parallel$  (see (A.45)) by the so-called *neoclassical* (Section 1.5.1) conductivity, one formula for which is (Wesson 2004, p. 174)

$$\hat{\sigma}_\parallel = g\sigma_\parallel, \quad (g \approx (1 - \varepsilon^{\frac{1}{2}})^2, \quad \varepsilon = r/R_0). \quad (1.16)$$

As will be explained in Section 2.4.4, the factor  $g$  is due to the trapping of particles between magnetic mirrors in the tokamak field, which reduces the number of electrons available to conduct electric currents. (In the rest of this text, we shall use  $\hat{\sigma}_\parallel$  and  $\hat{\eta}_\parallel = \eta/g$  to denote the 'trapped particle' values of the parallel conductivity and parallel resistivity.)

### 1.3 Global confinement times

Overall measures of the confinement properties of tokamaks are provided by the times taken for the whole of their mass, momentum, and energy to be lost in the absence of replacements. In the following we shall ignore the toroidal curvature, treating the cross-sections as having axial symmetry about the minor axis. Alternately, we could take poloidal averages to remove

the  $\theta$ -dependence of the variables, but to first-order in  $\varepsilon = r/R_0$  the results are the same. The most frequently used and important global confinement time is that for the plasma thermal energy. Before defining it, we need an appropriate form of the energy equation.

From the equation of plasma motion (see (A.3)),

$$\varrho \left\{ \frac{\partial}{\partial t} + \mathbf{v} \cdot \nabla \right\} \mathbf{v} + \nabla p = \mathbf{j} \times \mathbf{B},$$

where  $\varrho$  is the plasma density and  $\mathbf{v}$  is the fluid velocity, we find that

$$\mathbf{v} \cdot (\nabla p - \mathbf{j} \times \mathbf{B}) = \varrho \mathbf{v} \cdot \left\{ \frac{\partial \mathbf{v}}{\partial t} + \mathbf{v} \cdot \nabla \mathbf{v} \right\}. \quad (1.17)$$

Let  $v_D$  denote the radial velocity of the plasma, which with good plasma confinement, we expect to be quite small. In tokamaks the force lies in the radial direction and (1.17) shows that  $\mathbf{v} \cdot (\nabla p - \mathbf{j} \times \mathbf{B})$  is  $O(v_D^2)$ , small enough to be removed from the plasma energy equation defined in (A.29). Also the poloidal average of  $j_\theta E_\theta$  is zero, whence

$$\frac{\partial(\varrho u)}{\partial t} + \frac{1}{r} \frac{\partial}{\partial r} \{ r(\varrho h v_D + Q_r) \} = j_\varphi E_\varphi - \mathcal{L}, \quad (1.18)$$

where  $\varrho u$  ( $= \frac{3}{2} p$ ) and  $\varrho h$  ( $= \frac{5}{2} p$ ) are the internal energy and enthalpy densities,  $Q_r$  is the sum of the electron and ion heat fluxes and  $\mathcal{L}$  is the rate at which energy lost by radiation.

### 1.3.1 Energy confinement time

The total thermal energy in the torus is proportional to

$$W = \frac{1}{2\pi} \int \frac{3}{2} p dS = \int_0^a \frac{3}{2} k_B (n_e T_e + n_i T_i) r dr, \quad (1.19)$$

so if (1.18) is integrated over a plasma cross-section orthogonal to the minor axis, the result can be expressed

$$\frac{\partial}{\partial t} (\ln W) + \frac{1}{\tau_E} = \frac{1}{\tau_E^*} - \frac{1}{\tau_E^R}, \quad (1.20)$$

where

$$\tau_E \equiv W / [r(\frac{5}{2} p v_D + Q_r)]_{r=a}, \quad (1.21)$$

$$\tau_E^* \equiv W / \int_0^a j_\varphi E_\varphi r dr, \quad (1.22)$$

and

$$\tau_E^R \equiv W / \int_0^a \mathcal{L} r dr. \quad (1.23)$$

These expressions define the energy confinement time  $\tau_E$ , the energy replacement time  $\tau_E^*$ , and the radiation loss time  $\tau_E^R$ . In deriving (1.22) it is assumed that  $\tau_E^*$  is due only to ohmic heating,  $j_\varphi E_\varphi$ . With other methods of supplying thermal energy, the denominator on the right

hand side of (1.22) is modified to give the total power input. An apparent difficulty in the definition of  $\tau_E$  is that the denominator is evaluated at the limiter, where the variables will be sensitive to boundary conditions. A method of avoiding this strong local dependence will be given in Section 4.1.3.

The radiation losses vary considerably from one tokamak to the next, depending on the amount and type of impurities that have entered from the walls. With a relatively clean plasma the radiated power will lie between 10 and 20 per cent of the input power, but with contaminated plasmas,  $Z_{\text{eff}}$  can be 5 or larger, resulting in some 50 per cent or more of the input power being radiated. Impurity radiation typically peaks at temperatures less than 100 eV (Ashby and Hughes 1981), so that clean, hot plasmas radiate mostly from the peripheral regions. In these cases the radiation term in (1.18) can be neglected almost up to the limiter position. If steady conditions can be assumed, (1.20) gives

$$\tau_E = \frac{\tau_E^* \tau_E^R}{\tau_E^R - \tau_E^*}. \quad (1.24)$$

Values of  $\tau_E^*$  and, with more difficulty,  $\tau_E^R$ , can be deduced from observations, and a theory of the transport of energy and mass in tokamaks would enable  $\tau_E$  to be calculated. Allowing for the uncertainty in the observations, a satisfactory theory should yield values of  $\tau_E$  agreeing with the right-hand side of (1.24) to within a factor of about 2 for a wide range of tokamak conditions.

Besides giving correct values for the confinement time, a tokamak transport theory must also pass the more difficult test of giving the correct radial dependence for dependent variables like  $T_e$  and  $n_e$ . When the mass and thermal diffusivities are themselves complicated, non-linear functions of these variables, a particularly severe test for the theory is that the radial dependencies that it predicts for these diffusivities agree with the experimental distributions of these quantities, a issue to which we shall return in Section 4.1.2.

### 1.3.2 Electron-energy confinement time

In many tokamak experiments the ion temperature and density are poorly known and in these cases it is usual to introduce the electron analogues of  $\tau_E$  and  $\tau_E^*$ . The energy equation for the electron gas is (see (A.28)):

$$\frac{\partial}{\partial t}(\varrho_e u_e) + \nabla \cdot (\varrho_e h_e \mathbf{v}_e + \mathbf{Q}_e) = \mathbf{j} \cdot \mathbf{E} + \mathbf{v} \cdot (\nabla p_e - \mathbf{j} \times \mathbf{B}) + \mathcal{Q}_{ei} - \mathcal{L}_e,$$

where we have used the approximation  $\mathbf{v}_e = \mathbf{v} - \mathbf{j}/en_e$ , which follows from the definition of  $\mathbf{j}$  given in (A.11), the relation  $\mathbf{v} = (m_i \mathbf{v}_i + m_e \mathbf{v}_e)/(m_i + m_e)$  and  $m_e \ll m_i$ .

It follows from  $\nabla \cdot \mathbf{j} = 0$  and the assumed geometry that  $\partial j_r / \partial r = 0$ , so that  $v_{ir} = v_{er} = v_D$  (known as the *ambipolar* condition). From (1.17) and Dalton's law,  $p = p_i + p_e$ , we find that for the electron gas (1.18) is replaced by:

$$\frac{\partial(\varrho_e u_e)}{\partial t} + \frac{1}{r} \frac{\partial}{\partial r} \{r(\varrho_e h_e v_D + Q_{er})\} = j_\varphi E_\varphi - v_D \frac{\partial p_i}{\partial r} + \mathcal{Q}_{ei} - \mathcal{L}_e. \quad (1.25)$$

We also need the perfect gas law,  $p_e = n_e k_B T_e$ , where  $k_B$  is Boltzmann's constant<sup>3</sup>.

<sup>3</sup>There is a list of physical constants on page XV.

The electron time scales are:

$$\tau_{Ee} \equiv W_e / [r(\frac{5}{2}p_e v_D + Q_{er})]_{r=a}, \quad (1.26)$$

$$\tau_{Ee}^* \equiv W_e / \int_0^a j_\varphi E_\varphi r dr, \quad (1.27)$$

and

$$\tau_{Ee}^R \equiv W_e / \int_0^a \mathcal{L}_e r dr, \quad (1.28)$$

where

$$W_e = \int_0^a \frac{3}{2} k_B n_e T_e r dr. \quad (1.29)$$

However, the appearance of  $-v_D \partial p_i / \partial r$  and  $Q_{ei}$  on the right-hand side of (1.25) requires a knowledge of  $n_i(r)$  and  $T_i(r)$  for an accurate determination of  $\tau_E$ ; these terms are usually neglected, which is justified if approximate estimates are sufficient.

### 1.3.3 Particle confinement time

Balance of electron numbers gives

$$\frac{\partial n_e}{\partial t} + \frac{1}{r} \frac{\partial}{\partial r} (r n_e v_D) = S_e(r), \quad (1.30)$$

where  $S_e(r)$  is the electron number density source term. In the steady state this equation yields

$$\tau_p = \tau_p^*, \quad (1.31)$$

where

$$\tau_p \equiv \int_0^a n_e r dr / [r n_e v_D]_{r=a}, \quad (1.32)$$

is the plasma confinement time and

$$\tau_p^* \equiv \int_0^a n_e r dr / \int_0^a S_e r dr. \quad (1.33)$$

is the plasma replacement time.

The main problem in using (1.31) to test a theory of mass diffusivity lies in finding an estimate for  $S_e(r)$ . In clean plasmas  $S_e$  is largely due to the ionization of the working gas, which raises the problem of the distribution of the neutrals. In highly contaminated plasmas ionization of impurities is the main source of electrons, so a theory giving their distribution is required. Estimates of  $\tau_p^*$  can be made from observations of the response of the discharge to a brief puff of neutral gas admitted through a fast-acting valve. These difficulties are reflected in the fact that relatively few data are available for the particle replacement time; some of the early observations have been listed by Hugill (1983).

### 1.3.4 Momentum confinement time

Let the plasma be subject to a force density  $\mathbf{F}_b$  due to a beam of particles being injected from an outside source, then the momentum equation for the plasma as a whole reads (see (A.7))

$$\frac{\partial}{\partial t}(\rho \mathbf{v}) + \nabla \cdot (\rho \mathbf{v} \mathbf{v}) + \nabla p + \nabla \cdot \boldsymbol{\pi} = \mathbf{j} \times \mathbf{B} + \mathbf{F}_b.$$

The forces  $\mathbf{j} \times \mathbf{B}$  and  $\nabla p$  lie along  $\hat{\mathbf{r}}$ , where  $\hat{\mathbf{r}}$  is unit vector in the radial direction, therefore in the axi-symmetric geometry described earlier, this equation has the toroidal component,

$$\frac{\partial}{\partial t}(\rho v_\varphi) + \frac{1}{r} \frac{\partial}{\partial r}(r \rho v_r v_\varphi) + \nabla \cdot \boldsymbol{\pi} \cdot \hat{\boldsymbol{\varphi}} = \mathbf{F}_b \cdot \hat{\boldsymbol{\varphi}}, \quad (1.34)$$

where  $\hat{\boldsymbol{\varphi}}$  is unit vector in the toroidal direction. The toroidal momentum confinement and replacement times are:

$$\tau_\varphi = \mathcal{H}_\varphi \left\{ \int_0^a \nabla \cdot \boldsymbol{\pi} \cdot \hat{\boldsymbol{\varphi}} r dr + [r \rho v_r v_\varphi]_a \right\}^{-1}, \quad (1.35)$$

and

$$\tau_\varphi^* = \mathcal{H}_\varphi / \int_0^a \mathbf{F}_b \cdot \hat{\boldsymbol{\varphi}} r dr = \frac{2\pi^2 R_0^2 a^2 \mathcal{H}_\varphi}{\text{Beam torque}}, \quad (1.36)$$

where

$$\mathcal{H}_\varphi \equiv \int_0^a \rho v_\varphi r dr, \quad (1.37)$$

and the beam torque is about the major axis. Similar definitions can be given for the poloidal momentum time-scales. In the steady-state (1.34) has the integral  $\tau_\varphi = \tau_\varphi^*$ .

Collisions ensure that all ions have much the same toroidal speed, so that the Doppler shift of spectroscopic lines from various impurities can be used to determine  $v_\varphi$ . Estimates of the beam torque supplied to the plasma can be obtained by applying Monte Carlo methods to the beam particles, and then values of  $\tau_\varphi^*$  given by (1.36) may be used to check any theory yielding values for  $\tau_\varphi$ . Also, an approximate value of  $\tau_\varphi$  may be obtained directly by switching off the beam and determining the  $e$ -folding time,  $\tau_{s\varphi}$ , for  $v_\varphi$  to decay to ohmic collisional levels. With linear viscosity, we would expect  $\tau_{s\varphi} \approx \tau_\varphi$ , although this proves to be inaccurate (see Section 5.4.3).

## 1.4 Heating

A brief account of the various methods of heating tokamak plasmas is appropriate at this stage, since the central problem that will concern us later is the loss of this thermal energy at rates many times greater than initially predicted by the usual theories. Figure 1.2 indicates the magnitude of the heating task. Three types of heating are commonly used — ohmic heating (OH), neutral beam injection (NBI) and radio-frequency heating (RFH); unfortunately to date the temperatures achieved by these methods are somewhat lower than those required for ignition.

### 1.4.1 Ohmic heating

The experimental evidence in the early experiments (Hugill 1983) appeared to support the Spitzer formula for the parallel conductivity, which in a hydrogen plasma is (see (A.18))

$$\sigma_{\parallel} = 1.98 e^2 n_e \tau_e / m_e. \quad (1.38)$$

The validity of the neoclassical<sup>4</sup> factor  $g$  appearing in (1.16) is difficult to test in small tokamaks, but in Section 4.5.3 it will be shown that it increases the resistivity in JET by a factor of  $\sim 2.86$  and ohmic heating is similarly enhanced.

Provided the transformer action illustrated in Fig. 1.1 occurs on a time-scale long enough to permit the electric field to penetrate the plasma, it may be assumed that  $E_{\varphi}$  is approximately constant across the plasma cross-section. In this case the current profile can be deduced from the temperature profile, since by Ohm's law ( $j_{\varphi} = \sigma_{\parallel} E_{\varphi}$ ), (1.14) and (1.38) it follows that

$$j_{\varphi} \propto T_e^{3/2} / Z_{\text{eff}}. \quad (1.39)$$

The initial heating in tokamaks is due to ohmic dissipation of the toroidal current, which occurs at the rate,

$$P_{\Omega} = \hat{\eta}_{\parallel} j_{\varphi}^2 \quad (\hat{\eta}_{\parallel} \equiv \eta_{\parallel} / g) \quad (1.40)$$

per unit volume. While this is sufficient to achieve temperatures up to 1 keV or so, because  $\eta_{\parallel}$  is proportional to  $T_e^{-3/2}$ , it becomes inefficient at higher temperatures. An estimate for  $P_{\Omega}$  at the center of the plasma can be found from (1.12) and the approximation  $q_0 \approx 1$ ; thus with  $g \approx 0.35$  for JET (see Section 4.5.3),

$$P_{\Omega 0} = \hat{\eta}_{\parallel} \left( \frac{2B_{\varphi}}{\mu_0 R_0} \right)^2 \approx 0.20 \hat{T}_{e0}^{-3/2} (B_{\varphi} / R_0)^2 Z_{\text{eff}} \text{ MW m}^{-3}, \quad (1.41)$$

where  $\hat{T}_{e0}$  is the central temperature in keV.

This input power first heats the electrons, consequently for equilibrium it should balance the loss rate  $P_L \sim \frac{3}{2} k_B n_{e0} T_{e0} / \tau_{Ee}$ . Later (Section 4.1.3) we shall show that in low  $\beta_p$  plasmas,

$$\tau_{Ee} \approx 9.4 \times 10^{-22} \langle n_e \rangle a R_0^2 q_a \langle \hat{T}_e \rangle^{-1/2}, \quad (1.42)$$

where for circular cross-sections,

$$\langle n_e \rangle \equiv \frac{2}{a^2} \int_0^a n_e(r) r dr, \quad (1.43)$$

and

$$\langle T_e \rangle \equiv \frac{2}{\langle n_e \rangle a^2} \int_0^a n_e(r) T_e(r) r dr. \quad (1.44)$$

With typical profiles (see Section 4.1.1),  $n_{e0} \approx 2.25 \langle n_e \rangle$  and  $T_{e0} \approx 2.1 \langle T_e \rangle$ , therefore

$$P_L = 0.41 \frac{\hat{T}_{e0}^{3/2}}{a R_0^2 q_a} \text{ MW m}^{-3}. \quad (1.45)$$

<sup>4</sup>For a brief description of neoclassical transport see Section 1.5.1; a fuller account is given in Section 3.4.

Equating  $P_L$  and  $P_{\Omega 0}$  we arrive at the approximate relation

$$\hat{T}_{e0} \approx 0.79 (aq_a)^{1/3} B_\phi^{2/3} Z_{\text{eff}} \text{ keV}. \quad (1.46)$$

In JET, under typical ohmic heating conditions ( $a = 1.2$ ,  $q_a = 3$ ,  $B_\phi = 3$ ), this formula gives  $\hat{T}_{e0} \sim 2$  keV. A typical pre-1980 tokamak (Pfeiffer and Waltz 1979) has  $a = 0.2$ ,  $q_a = 5$ ,  $B_\phi = 3$ , and by (1.46),  $\hat{T}_{e0} \sim 1.6$  keV; these temperatures are similar to those obtained in experiments. The central temperatures are subject to considerable variations because of MHD instabilities and impurities, so (1.46) is not expected to be accurate, but at least it is sufficient to indicate the limitations of ohmic heating.

### 1.4.2 Neutral beam heating

When a beam of high-velocity neutral particles is injected into a tokamak plasma, it becomes ionized by charge exchange and particle collisions. The fast ions that result are then slowed down by Coulomb collisions, transferring most of their energy into electron thermal energy.

Let  $m_b$ ,  $v_b$ , and  $\xi_b = \frac{1}{2}m_b v_b^2$  denote the beam ion mass, velocity, and energy. The drag force  $F_{be}$  that the beam particles experience due to collisions with the electrons is  $m_b v_b / \tau_{be}$  where  $\tau_{be}$  is the slowing-down time for beam particles. The rate at which particle momentum is lost is proportional to the masses involved, thus  $\tau_b / \tau_e = m_b / Z m_e$ . Hence

$$\tau_{be} = \frac{m_b}{Z m_e} \tau_e \quad \left( \tau_e = \frac{2.75 \times 10^5 T_e^{3/2}}{\ln \Lambda Z n_e} \right). \quad (1.47)$$

The collision interval is only weakly dependent on the Coulomb logarithm  $\ln \Lambda$  and in evaluating  $\tau_e$  for application to tokamaks, we shall adopt the value  $\ln \Lambda = 17$  as being sufficiently accurate for typical temperatures and densities (see (A.17)).

The rate of energy loss is  $F_{be} v_b = 2\xi_b / \tau_{be}$  and therefore the electrons are heated at the rate  $\mathcal{P}_e = 2\xi_b / \tau_{be}$ . Evaluating the constant we get

$$\mathcal{P}_e = 1.71 \times 10^{-18} \frac{n_e \xi_b}{A_b \hat{T}_e^{3/2}} \text{ keV s}^{-1} \quad \left( \hat{T}_e, \xi_b \text{ in keV}, A_b \equiv \frac{m_b}{m_p} \right), \quad (1.48)$$

per beam ion.

Similarly, we find that the plasma ions are heated at the rate

$$\mathcal{P}_i = \frac{m_b}{m_b + m_i} \frac{2\xi_b}{\tau_{bi}} \approx 0.97 \times 10^{-17} \frac{n_i A_b^{1/2}}{A_i \xi_b^{1/2}}, \quad (1.49)$$

where the energy has been divided between the beam ions and the plasma ions inversely as their masses (cf. (A.24)) and the slowing-down time for a beam colliding with ions is given by (Spitzer 1962),

$$\tau_{bi} = \frac{m_b}{m_b + m_i} \frac{4\pi \epsilon_0^2 m_b m_i v_b^3}{n_i e^4 \ln \Lambda}. \quad (1.50)$$

Therefore

$$\mathcal{P}_i = 0.97 \times 10^{-16} \frac{n_i A_b^{\frac{1}{2}}}{A_i \xi_b^{\frac{1}{2}}} \text{ keV s}^{-1} \quad (\xi_b \text{ in keV}). \quad (1.51)$$

Let

$$\xi_c \equiv \frac{14.8 A_b \hat{T}_e}{(Z_i A_i)^{3/2}}, \quad (1.52)$$

then the sum of (1.48) and (1.51), i.e. the total plasma heating per beam ion, can be expressed

$$\mathcal{P} = 1.71 \times 10^{-18} \frac{n_e \xi_b}{A_b \hat{T}_e^{3/2}} \left( 1 + \left( \frac{\xi_c}{\xi_b} \right)^{\frac{3}{2}} \right) \text{ keV s}^{-1}. \quad (1.53)$$

When  $\xi_b = \xi_c$ , the electron and ion heating rates are equal.

Injection energies are usually greater than  $\xi_c$ , so at first the electrons are preferentially heated; as the beam ions slow down and  $\xi_b$  falls below  $\xi_c$ , it is the ions that receive most of the energy. The net effect is that the total electron heating and ion heating are comparable; ion temperatures over 15 keV have been achieved in JET by NBI.

To produce a neutral beam it is first necessary to charge the particles by ionization so that they can be accelerated by an electric field. Following this, they are neutralized by charge exchange. But there is a balance between the rates at which they are neutralized and re-ionized by collisions, so a completely neutral beam is not possible. Unfortunately, the ionized fraction in the beam increases rapidly with increasing beam energy, and since these beam ions would not penetrate the tokamak field, but would be deflected on to the walls of the injection port, they are removed magnetically from the beam and dumped; thus the beam efficiency falls off rapidly with beam energy. A reactor plasma might be over 2 m in radius (see Section 6.5.2), so for the beam to penetrate far enough to deposit the energy in the central regions implies a very inefficient beam.

### 1.4.3 Radio-frequency heating

Radio-frequency (RF) heating depends on the transfer of energy from electromagnetic waves generated by an external source to particles at suitable resonance frequencies. Resonance absorption of wave energy does not involve collisions and unlike ohmic heating, the process becomes more efficient with increasing temperature. A multi-species plasma in a magnetic field has several resonance frequencies capable of absorbing the energy of incident waves, and gradients in the number density and temperature mean that these resonances occur in narrow regions, admitting the possibility of localized heating and hence of some control over the temperature and current profiles across the minor cross-section. The cyclotron frequencies are defined in (A.33), viz.  $\omega_c = QB/m$ , where  $Q$  is the particle charge and  $m$  is its mass.

Ion-cyclotron resonance heating (ICRH) ( $\omega \sim \omega_{ci}$ ), lower hybrid resonance heating (LHRH), ( $\omega_{ce} < \omega < \omega_{ci}$ ) and electron-cyclotron resonance heating (ECRH) ( $\omega \sim \omega_{ce}$ ) have proved to be the most successful of the RF experiments, and temperatures have been raised substantially (up to 5 keV). Lower hybrid resonance has been used in JET to modify the current distribution by what is termed ‘‘current drive’’. The waves are directed along the

field lines and absorption takes place by Landau damping (e.g. see Woods 2004, p. 123) of those plasma electrons that have a parallel velocity similar to the phase velocity.

The theory of these high-frequency waves and their absorption by Landau damping is an extensive and much researched subject, but falls outside the range of this introductory text; Porkolab (1979) has written a general survey, and Wesson (2004) gives a review with many references.

## 1.5 Electron energy confinement time

### 1.5.1 Ohmically-heated tokamaks

A large number of early experiments concerned with transport in tokamaks has been reported, mainly in the journal *Nuclear Fusion*. Hugill's review lists 237 papers and deals almost entirely with ohmically-heated discharges (Hugill 1983). The observations reveal two regimes, corresponding to low and high beta plasmas with continuous variation between. In the pre-1980 and mainly low beta tokamaks, the empirical scaling laws inferred from observations were simple, with confidence about the linear dependence of  $\tau_{Ee}$  on the line averaged density  $\bar{n}_e$  defined in (1.56), but not much else; this situation has changed and now there is general agreement about the dependence of  $\tau_{Ee}$  on all the major plasma parameters in the low beta regime.

#### Neoclassical transport

We shall refer to 'neoclassical' transport several times before reaching Section 3.1.4 and Section 3.4, where the physical basis of the phenomenon will be discussed in detail. For the present the following remarks will serve to identify the distinction implied by the prefix 'neo'.

By 'classical transport' is meant the diffusion of some property through the plasma carried by individual ions or electrons moving under the usual Lorentz force, without any disturbance of their orbits by turbulence or instabilities. Fourier's law for the diffusive transport of energy is a good example:

$$\mathbf{q} = -\boldsymbol{\kappa} \cdot \nabla T, \quad (1.54)$$

where  $\boldsymbol{\kappa}$  is the thermal conductivity tensor, whose structure is described in Section A.7. The classical value of  $\boldsymbol{\kappa}$  can be derived from kinetic theory. Particles move through a mean free path (the displacement between successive collisions) and then pass on their excess energy by colliding with particles that have arrived from a cooler part of the plasma. In a direction normal to strong magnetic fields, the mean free paths are just twice the Larmor radius (see Fig. A.2), so transport is considerably inhibited by the limited displacements possible.

Diffusive transport is very different from convective transport in which it is the bodily movement of *fluid* elements that moves (convects) the energy through the plasma. Both kinds of transport are evident in equation (1.26), in which the term  $\frac{5}{2}p_e v_D$  is due to the convection of electron energy, while  $Q_{er}$  represents the diffusion of electron thermal energy.

Neoclassical transport differs from classical transport in that for many particles rather large displacements are possible during their transit between collisions. These particles are

trapped in the tokamak magnetic fields and as a consequence trace rather large, banana-shaped orbits whose widths are many times greater than a Larmor radius; this phenomenon increases the cross-field transport of heat and momentum to values several hundred times the classical value. Neoclassical transport was once considered to be the explanation for the rapid loss of heat from tokamaks, which occurs hundreds of times faster than early expectations based on the classical theory. However, tokamak losses exceed those predicted by neoclassical theory by roughly two orders of magnitude, so attention has turned to turbulent transport to explain both energy and particle losses. We shall discuss these problems in more detail in Chapter 3.

### (i) Low beta regime

With ohmic heating it became standard practice to express  $\tau_{Ee}$  in the form

$$\tau_{Ee} = 10^{-\alpha} \bar{n}_e^{\alpha_n} a^{\alpha_a} R_0^{\alpha_R} q_a^{\alpha_q} \langle T_e \rangle^{\alpha_T} Z_{\text{eff}}^{\alpha_Z} \dots, \quad (1.55)$$

where the indices  $\alpha, \alpha_n, \alpha_a, \dots$  are chosen to obtain the best statistical fit for a wide range of observations. The density-averaged temperature  $\langle T_e \rangle$  used above is defined in (1.44); for density, instead of the volume-averaged density defined in (1.43), it is usual to adopt the line-averaged density defined by

$$\bar{n}_e \equiv \frac{1}{a} \int_0^a n_e dr, \quad (1.56)$$

which is more closely related to actual observations.

Of course there is no a priori reason why (1.55) should be the correct form and later (in Section 4.2) we shall find from a theoretical approach that a *sum* of two terms is required to explain the functional dependence of  $\tau_{Ee}$ . The statistical approach predates the existence of a reliable theory and in fact now provides a useful test that any proposed theory should pass.

One variable surprisingly absent from (1.55) is the magnetic field strength  $B$ , but out of a dozen empirical scaling laws of this type reported by Hugill (1983), only one involved  $B$ , and in any case (1.10), viz.  $q_a = 5a^2 B_\varphi / \hat{I}_p R_0$ , could have been used to remove  $B_\varphi$  in favor of the plasma current and the variables already appearing in (1.55).

To determine the indices is not straightforward, since it is rarely possible to vary the parameters one at a time. Furthermore, with steady-state, ohmically-heated tokamaks, the temperature cannot be externally controlled, and as both  $\tau_{Ee}$  and  $\tau_{Ee}^*$  in (1.26) and (1.27) depend on  $T_e$ , the scaling of  $\tau_{Ee}^*$  with  $T_e$  masks the confinement time scaling. In principle this ambiguity could be overcome with the help of additional non-ohmic heating, but if this additional heating is dominant, a new independent variable, the input power  $P$ , must be added to the list and again the temperature dependence is obscured. However, if the radiation losses are negligible, the value of  $\alpha_T$  in (1.55) can be deduced by dimensional analysis. For this we need the theorem given in Section A.5, which allows us to write (1.55) in the form,

$$B\tau_{Ee} \propto (\bar{n}_e a^2)^{\alpha_n} (\langle T_e \rangle a^{1/2})^{\alpha_T} B a^{5/4} q_a^{\alpha_q} (R_0/a)^{\alpha_R} Z_{\text{eff}}^{\alpha_Z} a^{(\alpha_a + \alpha_R - 2\alpha_n - \alpha_T/2 - 5/4)}$$

and since the dimensional term  $a^{(\dots)}$  cannot appear, we deduce that

$$\alpha_T = 2(\alpha_a + \alpha_R - 2\alpha_n - \frac{5}{4}). \quad (1.57)$$

**Table 1.2:** Power law indices for  $\tau_{Ee}$ 

| Experiment <sup>†</sup> | $\alpha$ | $\alpha_n$ | $\alpha_a$ | $\alpha_R$ | $\alpha_q$ | $\alpha_Z$ | $\alpha_T$ | $\alpha_T^*$ |
|-------------------------|----------|------------|------------|------------|------------|------------|------------|--------------|
| 1                       | 19.02    | 0.90       | 0.98       | 1.63       | —          | 0.23       | —          | -0.88        |
| 2                       | 18.44    | 1          | 2          | —          | 0.75       | —          | —          | —            |
| 3                       | 20.46    | 1          | 0.25       | 2.75       | 1          | —          | -0.5       | -0.5         |
| 4                       | —        | 1          | 1          | 2          | 1          | —          | —          | -0.5         |
| 5                       | 20.3     | 1          | 2          | 1          | 0.5        | —          | —          | -0.5         |
| 6                       | —        | 1.15       | —          | —          | 0.9        | —          | —          | —            |
| 7                       | 21       | 1          | 1.04       | 2.04       | 0.5        | —          | —          | -0.34        |
| ‘ideal’                 | —        | 1          | 1          | 2          | 1          | —          | -0.5       | —            |

<sup>†</sup>1. Pfeiffer & Waltz (1979); 118 observations on 11 tokamaks. 2. Ejima et al. (1982); Doublet III. 3. Merezhkin (see Lenov et al. (1980)); T11. 4. Efthimion et al. (1984); TFTR. 5. Equipe TFR (1980); mainly TFR. 6. Cordey et al. (1985a); JET. 7. Goldston (1984); results combined from 12 tokamaks.

Table 1.2 lists the values of the indices obtained for a wide range of tokamak variables. When an integer value was clearly indicated by the observations, this was chosen by some authors even though not quite statistically optimal. Only one group ventured a value for  $\alpha_T$ ; this was obtained indirectly, via an experimental determination of the thermal diffusivity. In the earlier experiments the dependence on  $q_a$  was not clear, but recent JET measurements give  $\alpha_q = 0.9 \pm 0.1$ , supporting the value of unity obtained on T11 and TFTR shown in Table 1.2.

The values of  $\alpha_T^*$  in the last column were not given in the papers quoted; they are our dimensional analysis values given by (1.57). The earlier tokamaks, featured in Pfeiffer and Waltz’s numerical study, lost about half their energy by radiation, which accounts for their relatively high adverse scaling with temperature ( $\alpha_T^* = -0.88$ ). At the bottom of Table 1.2, the row marked ‘ideal’ gives the values of the indices that we would expect to appear in an exact theory of electron thermal transport, at least for the density range represented in the table. The fact that statistical analysis yields numbers for the indices close to integer values suggests the existence of an under-pinning theory that is unlikely to involve the chaos of turbulence. It is this theory that shall be developed in later chapters. No ‘ideal’ value for the index  $\alpha$  of the numerical coefficient is possible, for as we will see later, this number depends on the temperature and density profiles.

The above description applies to  $\tau_{Ee}$ , but  $\tau_E$  is bound to follow a similar pattern, being typically about 50% or so longer. In early experiments the ions reached about half the electron temperature, which implied that although the electrons provided the dominant loss mechanism, the losses through the ions were also somewhat larger than predicted by the early theories. Convective energy losses are complications that will be treated later; it is usual to treat these losses as being negligible, but the experimental evidence for this is not clear.

## (ii) High beta regime

At high densities it was discovered that the empirical law  $\tau_E \propto \bar{n}_e$  overestimated  $\tau_E$ , and a weaker dependence was required (Gaudreau et al. 1977, Equipe TFR 1980). And at higher

densities still,  $\tau_E$  reaches a flat maximum and then starts to fall as  $\bar{n}_e$  is increased (Ejima et al. 1982). Figure 1.8 shows an example of the ‘saturation’ of  $\tau_E$  with increasing values of  $\bar{n}_e q_a$  in TFTR (Efthimion et al. 1984).

Since higher density means an increase in collision frequency, it was presumed (Alladio et al. 1982) that neoclassical transport — in particular ion conductivity — was responsible for the saturation of  $\tau_E$ . But some observations had ion conduction losses several times larger than neoclassical values (Ejima et al. 1982). It is not clear from the observations that ion transport is the cause of the additional losses. Goldston (1984) noted similarities in the energy confinement between the high beta regime and the L-mode (see Section 1.5.2) for neutral beam heating. He correctly speculated that the same transport processes might well be operating in each case and as the losses in beam-heated plasmas are known to be dominated by electron transport, electron losses should also be dominant in the high beta regime.

In Section 4.3.2 it will be shown that in the L-mode

$$\tau_{Ee} = \frac{0.5}{1 + 2.13\beta_p} \frac{\mu_0 e^2}{(2m_e)^{\frac{1}{2}}} \frac{\bar{n}_e a R_0^2 q_a}{\langle k_B T_e \rangle^{\frac{1}{2}}},$$

where from (1.6) and (1.10)

$$\beta_p = \frac{2R_0^2}{a^2} \frac{\mu_0 \langle p \rangle}{B_\varphi^2} q_a^2 \propto \frac{\bar{n}_e q_a^2}{a^2}.$$

Hence at a fixed values of  $B_\varphi$  and temperature,

$$\tau_{Ee} \propto \frac{(a^2/q_a)\beta_p}{1 + 2.13\beta_p},$$

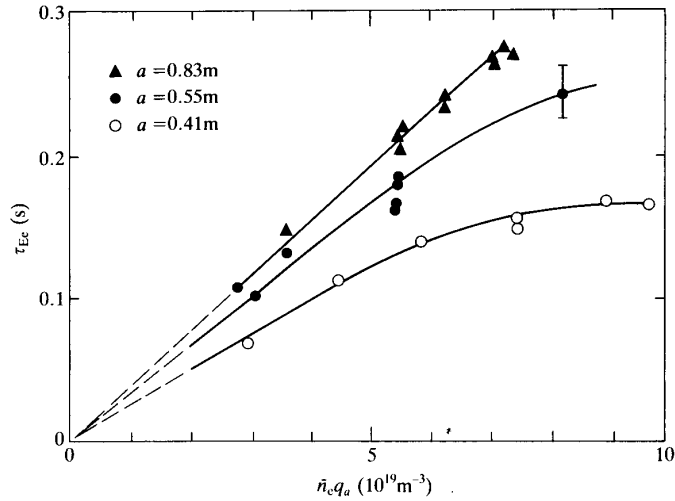


**Figure 1.8:** Total energy confinement time in TFTR

showing that the electron energy confinement time, considered as a function of poloidal beta, saturates when  $\beta_p \gg 0.47$ , which implies the existence of a similar constraint on  $\bar{n}_e q_a$  as indicated in Fig. 1.8. An important conclusion is that we cannot expect to find an accurate *single* term formula like (1.55) for  $\tau_{Ee}$  over the whole of the accessible  $\beta_p$  range.

### 1.5.2 Auxiliary heated plasmas

By ‘auxiliary’ heating is meant either neutral beam injection (NBI) or radio-frequency heating (RFH). One might expect the transport of energy from a magnetoplasma to be independent of the method of heating, but it appears that this is not so in tokamaks. As the auxiliary heating is increased from zero to levels much higher than the ohmic heating (OH), the energy confinement time  $\tau_E$  changes from the function in (1.55) to a rather different one; furthermore, with NBI the electrons remain the dominant energy loss channel. The implication is that either the electron thermal conductivity depends on the method of heating, or more likely, that some other mechanism involving electrons becomes important. Compared with ohmic heating, RF heating has the advantages of providing the off-axis current drive required to maintain plasma stability, and of giving direct ion heating; it also has the merit of generating small ELMs (see Section 6.4.2). For a review of this topic see ITER team (1999), Chapter 6.

A surprising distinction between tokamaks with divertors and those with limiters was discovered (Wagner et al. 1982a,b), namely that with NBI those discharges with divertors were able to contain particles and energy for about twice as long as was possible in the same conditions with normal ‘limiter’ discharges; this first regime is termed the ‘H’ (high) mode of operation while the second usual limiter discharge is referred to as the ‘L’ (low) mode. Limiter discharges have also been made to perform in the H-mode by injecting a small amount of neon (termed ‘neon puffing’) (Lazarus et al. 1985). It is evident that confinement with auxiliary heating is quite sensitive to the boundary conditions; it is now accepted that the essential feature for H-mode operation is that there is a reduction in neutral recycling in the main plasma. Why this should increase  $\tau_E$  will be discussed shortly.

#### (i) The L-mode

In the L-mode the observations from several tokamaks are in broad agreement with the empirical law:

$$\tau_E = 3.7 \times 10^{-5} I_p^v P_b^w R_0^x a^y, \quad (1.58)$$

where  $I_p$  is the plasma current and  $P_b$  is the total beam power absorbed by the plasma. From the relatively few observations available at the time, Goldston (1984) obtained the estimates

$$v = 1, \quad w = -0.5, \quad x = 1.75, \quad y = -0.37. \quad (1.59)$$

Note that the energy replacement time for  $P_b$  is (cf. (1.19) and (1.22)),

$$\tau_E^* = 3\pi^2 R_0 a^2 k_B \{ \langle n_i \rangle \langle T_i \rangle + \langle n_e \rangle \langle T_e \rangle \} / P_b. \quad (1.60)$$

Dimensional analysis yields the relation

$$B\tau_E = F(\bar{n}a^2, I_p/P_b^{1/3}, I_p/(aB), \beta, R_0/a, Z_{\text{eff}}) \quad (1.61)$$

for the energy confinement time, and when this is applied to (1.58) the constraints

$$v + 3w + 1 = 0, \quad x + y = 1, \quad (1.62)$$

are obtained. Considering the possible errors involved, Goldston's values are satisfactory. Neilson et al. (1983) found that for the ISX tokamak at Oak Ridge, USA,  $v = 2/3$  and  $w = -2/3$ , values that are similar to Goldston's.

With auxiliary heating there appears to be little, if any, dependence of  $\tau_E$  on either  $\bar{n}_e$  or  $B$ . Since the number of Coulomb collisions per unit path length — termed the 'collisionality' — scales as  $\bar{n}_e T^{-2}$ , collisions are clearly not the cause of the loss of energy. If turbulence is assumed to be responsible the process must be independent of  $\bar{n}_e$ , which rules out several types of turbulence.

With OH plasmas  $\tau_E$  depends on  $\bar{n}_e$ , whereas with NBI plasmas it does not; therefore when both forms of heating are present two separate processes are required to explain the phenomenon.

### (ii) The H-mode

There is no consensus about the scaling law in the H-mode. Some research groups find that  $\tau_E$  scales as in the L-mode, except that its magnitude is increased substantially. Others have found scalings similar to OH plasmas, or intermediate scalings involving both  $\bar{n}_e$  and  $I_p$ . A successful tokamak reactor will probably need to operate in the H-mode, although the improvement in confinement is offset by an increase in impurity level and by the appearance of an instability known as an edge localized mode (ELM) explained in Section 6.4.2.

One clue to the H-mode phenomenon is the observation that limiter plasmas can be switched into the H-mode by neon-puffing, and that this increases both  $\tau_E$  and the particle confinement time  $\tau_p$  (Lazarus et al. 1985). It appears that convection is being inhibited, and that the boundaries are being partially thermally insulated from the body of the plasma. The collision cross-section between the plasma ions and the introduced impurities is relatively high, so the neon impedes their radial flow, especially near the boundary; with divertors convection is naturally lower because of the absence of neutrals recycling into the tokamak plasma. These two observations suggest that the distinction between L-mode and H-mode plasmas depends on the thermal boundary condition at the edge of the magnetoplasma; the L-mode requires good thermal contact, whereas the H-mode depends on this contact being somewhat reduced.

The continuous injection of small, frozen hydrogen isotope pellets is the favored method of particle refueling for the next generation of tokamaks, since this allows both deeper refueling and better profile control than with gas puffing. It is found that the plasma that results after pellet injection has different transport properties from the initial plasma (Hugon et al. 1992), and the tokamak operates in what is termed a *pellet enhanced performance* (PEP) mode. For example pellet injection can switch a limited L-mode plasma into an H-mode and increase the energy confinement time by a factor  $\sim 3$  (see Section 6.4.4).

### 1.5.3 Profile shapes and energy losses

Changes in the shape of the temperature profile can be effected by adding metallic impurities, and increasing the radiation losses. With sufficient impurities hollow profiles are obtained, and the resulting values of  $\tau_E$  are quite low. A moderate impurity level gives broad profiles

and improved values for  $\tau_E$ , whereas low impurity levels give peaked profiles and the highest values of  $\tau_E$ . These changes in  $\tau_E$  occur when the gross parameters of the discharge are similar. Factors up to 4.6 in  $\tau_E$  due to profile alteration alone, have been reported (Meservey et al. 1976). Profiles that are found to be in fair agreement with observations at low poloidal beta are:

$$T_e = T_{e0}(1 - y)^{\alpha_t}, \quad n_e = n_{e0}(1 - y)^{\alpha_n} \quad (y = (r/a)^2),$$

where the constants  $\alpha_n$  and  $\alpha_t$  usually fall in the ranges (0.6, 1.5) and (1.5, 3) respectively. Pfeiffer and Waltz's (1979) list of observations for ohmically heated plasmas have average values for  $\alpha_t$  and  $\alpha_n$  of 2.5 and 1.25 with a considerable spread.

With strong NBI heating, the additional heating and refueling in the central regions tends to steepen both the density and temperature profiles. A distinction can be made between tangential co-injection (beam parallel to the toroidal current and tangential counter-injection (beam anti-parallel).

In purely OH-discharges it is found that in the central region the plasma mass flows in a direction opposing the current, and in the peripheral region it flows with the current. (Suckewer et al. 1981; Brau et al. 1983). This description applies to the ion component of the plasma, hence, with co-injection the velocity of the beam particles relative to the plasma particles will be less in the central regions than with counter-injection. By (1.48) and (1.49) co-injection will result in more rapid heating of the central plasma and hence steeper temperature profiles. To anticipate Table 5.3, this means smaller values of  $\tau_p$  with co-injection than with counter-injection, a phenomenon that has been observed on the ISX-B tokamak (Scott et al. 1985).

#### 1.5.4 Disruptive instabilities

There is one remarkable phenomenon that should be mentioned in this introductory chapter. It is the quite sudden changes that can occur in the basic macroscopic variables like temperature, number density and the safety factor. By "sudden" is meant substantial changes that can occur in times of the order of a few electron collision intervals, which by (1.14) for the typical JET values:  $Z_{\text{eff}} = 2$ ,  $n_e = 2 \times 10^{19} \text{ m}^{-3}$ ,  $T_e = 2 - 6 \text{ keV}$  is 45 - 200  $\mu\text{s}$ . This means that local thermodynamic equilibrium is almost lost during these aptly named *disruptions*.

There are two main types of disruption: first there is a *minor* disruption from which the temperature is restored to its original value, evolving along a 'ramp phase' that for JET takes about 40 to 100 micro-seconds to complete. In this case the profile has a sawtooth appearance, with the ramp phase about 500 times longer than the collapse phase. These sawtooth oscillations appear so regularly that they are interpreted as an indication that the discharge is behaving normally. Figure 1.9 shows three distinct types of collapse precursors; in Fig. 1.9(a) the oscillations preceding the sudden collapse have period of about 120  $\mu\text{s}$  and the collapse itself occurs on the same time-scale, so there appears to be a close relationship between the 'over-stable' precursor oscillations and the final collapse.

In certain circumstances, described as being near the *density limit*, there is a sudden collapse from which recovery does not occur. In this case the sawtooth oscillations that usually precede a minor disruption do not occur, and the phenomenon is termed a *major disruption*, which releases a lot of electromagnetic energy in a chaotic fashion that could seriously damage the tokamak structure and therefore they are usually avoided. As will be shown in Sec-

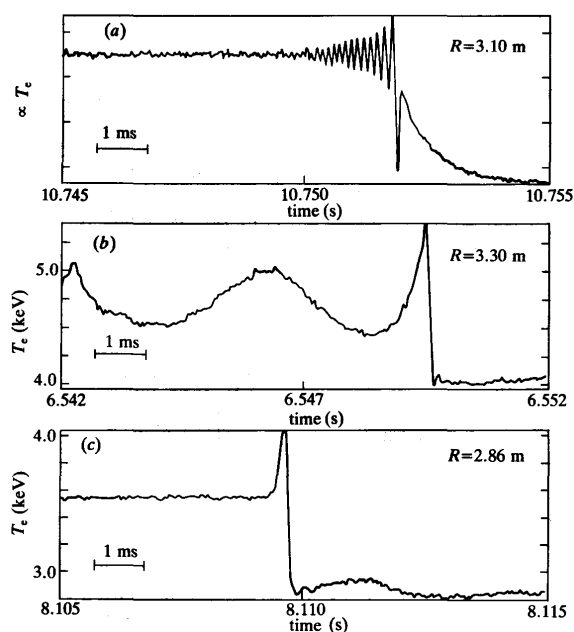


**Figure 1.9:** Three types of minor disruption in JET (in (a) the ordinate is proportional to  $T_e$ )

tion 6.2.1, there are two circumstances that give rise to these severe instabilities, (i) there is a 'low  $q_a$ ' limit and (ii) a 'density limit'. This upper bound to  $n_e$  affects the ignition condition in (1.1) and could make tokamaks economically unviable.

## References

Abbreviations for conference proceedings:

|  |      |
|--|------|
| <i>Plasma Physics and Controlled Nuclear Fusion Research</i>           |      |
| 1em (Proc. 7th Int. Conf., Innsbruck, 1978) IAEA Vienna                | O    |
| (Proc. 8th Int. Conf., Brussels, 1980) IAEA Vienna                     | I    |
| (Proc. 10th Int. Conf., London, 1984) IAEA Vienna                      | II   |
| <i>Current Disruption in Toroidal Devices</i>                          |      |
| Proc. IAEA Tech. Committee Meeting, Garching; Feb. 1979, Rep. IPP-3/51 | III  |
| <i>European Conference on Controlled Fusion and Plasma Physics</i>     |      |
| (Proc. 7th European Conf., Lausanne, 1975)                             | IV   |
| (Proc. 12th European Conf., Budapest, 1985)                            | V    |
| (Proc. 11th Int. Conf., Kyoto, 1986)                                   | VI   |
| (Proc. 13th Int. Conf., Washington, 1990)                              | VII  |
| (Proc. 16th Int. Conf., Montreal, 1996)                                | VIII |

- Ashby, D. E. T. F. & Hughes, M. H. (1981). *Nuclear Fusion*, **21**(8), 911–26.
- Brau, K. (1983). *Nuclear Fusion*, **23**(12), 1643.
- Christiansen, J. P. et al. (1985). V, Pt I, 327.
- Cordey, J. G. et al. (1985a). V, Pt 1, 167.
- Cordey, J. G. et al. (1985b). V, Pt 1, 26.
- Denne, B. et al. (1985). V, Pt 1, 379.
- Efthimion, P. C. et al. (1984). II, Paper A-I-2.
- Ejima, S. et al. (1982). *Nuclear Fusion*, **22**(12), 1627–49.
- Equipe TFR (1980). *Nuclear Fusion*, **20**(10), 1227–45.
- Gaudreau, M. et al. (1977). *Phys. Rev. Lett.*, **39**(20), 1266–70.
- Goldston, R. J. (1984). *Plasma Physics and Controlled Fusion*, **26**(1A), 87.
- Hugill, J. (1983). *Nuclear Fusion*, **23**(3), 331–73.
- ITER team (1999). *Nuclear Fusion*, **39**(12), Ch. 6.
- JET team (1990). *Plasma physics and controlled fusion*, **32**, 837.
- Lawson, J. D. (1957). *Proc. Phys. Soc.*, **B 70**, 6.
- Lazarus, B. A. et al. (1985). *Nuclear Fusion*, **25**(2), 135–49.
- Lenov, V. M. et al. (1980). I, Vol. I, 393–403.
- Matthews, G.F. et al. (1997). *J. Nucl. Mater.*, **241–243**, 450.
- Meservey, E. B., Bretz, N., Dimock, D. L., & Hinnov, E. (1976). *Nuclear Fusion*, **16**, 593.
- Neilson, G. H. et al. (1983). *Nuclear Fusion*, **23**(3), 285–94.
- Pfeiffer, W. & Waltz, R. E. (1979). *Nuclear Fusion*, **19**, 51.
- Porkolab, M. (1979). In *Theory of confined plasmas*. Pergamon Press, Oxford.
- Rutherford, P. H. (1980). *Nuclear Fusion*, **20**(9), 1086–92.
- Scott, S. D. et al. (1985). Private communication, PPL, Princeton, N.J.
- Spitzer, L. (1962). *Physics of fully ionized gases*, 2nd edn. Interscience, New York.
- Suckewer, S. et al. (1981). *Nuclear Fusion*, **21**(10), 1301–09.
- Wagner, F. et al. (1982a). *Phys. Rev. Lett.*, **49**, 1408.
- Wagner, F. et al. (1982b). *Plasma physics and controlled nuclear fusion research*, IAEA-CN-41/A-3. IAEA, Vienna.
- Wesson, J.A. (2004). *Tokamaks*, 3rd edn. Oxford University Press.
- Woods, L.C. (2004). *Physics of plasmas*, Wiley-VCH Verlag GmbH & Co., KGaA, Weinheim.